Spatiotemporal intermittency and scaling laws in the coupled sine circle map lattice

Zahera Jabeen* and Neelima Gupte†
Indian Institute of Technology-Madras, Chennai, India
(Received 18 April 2006; published 27 July 2006)

We study spatiotemporal intermittency (STI) in a system of coupled sine circle maps. The phase diagram of the system shows parameter regimes with STI of both the directed percolation (DP) and non-DP class. STI with synchronized laminar behavior belongs to the DP class. The regimes of non-DP behavior show spatial intermittency (SI), where the temporal behavior of both the laminar and burst regions is regular, and the distribution of laminar lengths scales as a power law. The regular temporal behavior for the bursts seen in these regimes of spatial intermittency can be periodic or quasiperiodic, but the laminar length distributions scale with the same power law, which is distinct from the DP case. STI with traveling wave laminar states also appears in the phase diagram. Solitonlike structures appear in this regime. These are responsible for crossovers with accompanying nonuniversal exponents. The soliton lifetime distributions show power-law scaling in regimes of long average soliton lifetimes, but peak at characteristic scales with a power-law tail in regimes of short average soliton lifetimes. The signatures of each type of intermittent behavior can be found in the dynamical characterizers of the system viz. the eigenvalues of the stability matrix. We discuss the implications of our results for behavior seen in other systems which exhibit spatiotemporal intermittency.

DOI: 10.1103/PhysRevE.74.016210 PACS number(s): 05.45.Ra, 05.45.Df, 64.60.Ak

I. INTRODUCTION

The phenomena of spatiotemporal intermittency (STI), wherein laminar states which exhibit regular temporal behavior co-exist in space and time with burst states of irregular dynamics, is ubiquitous in both natural and experimental systems. Such behavior has been seen in experiments on convection [1,2], counterrotating Taylor-Couette flows [3], oscillating ferrofluidic spikes [4], experimental and numerical studies of rheological fluids [5,6], and in experiments on hydrodynamic columns [7]. In theoretical studies, STI has been seen in partial differential equations such as the damped Kuramoto-Sivashinsky equation [8] and the one-dimensional Ginzburg-Landau equation [9], in coupled map lattices (CMLs) [10] such as the Chaté-Manneville CML [11], the inhomogeneously coupled logistic map lattice [12], and in cellular automata studies.

A variety of scaling laws have been observed in these systems. However, there are no definite conclusions about their universal behavior. The type of spatiotemporal intermittency in which a laminar site becomes active (turbulent) only if at least one of its neighbors is active has been conjectured to belong to the directed percolation (DP) universality class [13]. The dry state or the absorbing state in DP is identified with the laminar state in STI, and the wet state of DP corresponds to the active state in STI, with time as the directed axis. However, a CML specially designed to exhibit STI by Chaté and Manneville showed critical exponents significantly different from the DP universality class [11]. This led to a long debate in the literature [14–17]. It was concluded that the presence of coherent structures, called solitons, were responsible for spoiling the analogy with DP. The nature of the transition to STI and the identification of the universality classes of STI is still an unresolved issue, and is a topic of current interest.

Earlier studies of the diffusively coupled sine circle map lattice showed regimes of STI which were completely free of solitons [17,18]. Two types of STI were seen along the bifurcation boundaries of the bifurcation from the synchronized solution. The first type of STI showed an entire set of static and dynamic scaling exponents which matched with the DP exponents, and therefore was seen to belong convincingly to the DP class. The other type of intermittency, where both the laminar and burst regions showed regular temporal dynamics, was called spatial intermittency (SI). The laminar length distribution for this case showed characteristic power-law behavior with its own characteristic exponent $\zeta=1.1$. This kind of behavior has been observed in the sine circle map lattice as well as in the inhomogeneously coupled logistic map lattice. In the case of the sine circle map lattice, both types of intermittency, viz. STI of the DP class, and SI which does not belong to the DP class, were seen in different regions of the phase diagram. Moreover, distinct signatures of the two types of behavior were picked up by the dynamical characterizers of the system, i.e., the eigenvalues of the stability matrix. The eigenvalue spectrum was continuous in the DP regime, but exhibited the presence of gaps in the SI regime.

Different types of behavior are seen within the SI class itself. The laminar state is synchronized in nature, but the burst state can be periodic or quasiperiodic in its dynamical behavior. The periodic burst states can have different temporal periods. Burst states of the traveling wave type are observed at several points in the phase diagram. The distribution of laminar lengths shows power-law scaling in both cases with the same exponent.

The SI regimes lie close to the bifurcation boundaries of the synchronized solutions. The SI with traveling wave (TW) bursts bifurcates further via tangent-period doubling bifurcations, to STI with TW laminar states and turbulent bursts. This type of STI is contaminated with coherent structures

*Electronic address: zahera@physics.iitm.ac.in
†Electronic address: gupte@physics.iitm.ac.in

similar to the solitons that spoil the DP regime in the Chaté-Manneville CML. The solitons induce crossover behavior and the exponents in this regime take nonuniversal values. The distribution of soliton lifetimes shows two characteristic regimes. In the short soliton lifetime regime, the distribution shows a peak which indicates the presence of a characteristic time scale, and has a power-law tail. In the longer soliton lifetime regime, the distribution has no characteristic scale and shows pure power-law behavior. The solitons in this regime also change the order of the phase transition in the system.

The dynamical characterizers of the system show signatures of the different types of temporal behavior of the burst states. As mentioned earlier, the eigenvalue distribution of the stability matrix is gapless for the STI with DP exponents, whereas distinct gaps are seen in the distribution for the SI class. The number of gaps in the eigenvalue distribution of SI as a function of bin size shows power-law behavior. However, the scaling exponent is different for SI with quasiperiodic bursts and SI with periodic bursts. We discuss the implications of our results for behavior seen in other systems which exhibit spatiotemporal intermittency.

The organization of this paper is as follows. Section II gives the details of the model and the phase diagram obtained. The two universality classes of spatiotemporal intermittency seen in this system, as well as the variations within the SI class, are discussed in Sec. III. Section IV explains the role played by the solitons in inducing a crossover behavior in STI with traveling wave laminar state. The signatures of each type of intermittent behavior is seen in the dynamical characterizers of the system. This has been discussed in Sec. V. We conclude with a discussion of these results and their implications for other systems.

II. MODEL AND THE PHASE DIAGRAM

The coupled sine circle map lattice is defined by the evolution equations

$$x_i^{t+1} = (1-\epsilon) f(x_i^t) + \frac{\epsilon}{2}[f(x_{i-1}^t) + f(x_{i+1}^t)], \quad (\mathrm{mod}\ 1), \quad (1)$$

where $i=1,\ldots,N$ and t are the discrete site and time indices, respectively, with N being the size of the system, and ϵ being the strength of the coupling between the site i and its two nearest neighbors. The local on-site map, $f(x)$ is the sine circle map defined as

$$f(x) = x + \Omega - \frac{K}{2\pi}\sin(2\pi x). \quad (2)$$

Here, K is the strength of the nonlinearity and Ω is the winding number of the single sine circle map in the absence of the nonlinearity. The coupled sine circle map lattice has been known to model the mode-locking behavior [19] seen commonly in coupled oscillators, Josephson Junction arrays, etc., and is also found to be amenable to analytical studies [20]. The phase diagram of this system is highly sensitive to initial conditions due to the presence of many degrees of freedom. Studies of this model for several classes of initial conditions have yielded rich phase diagrams with many distinct types of attractors [19,20].

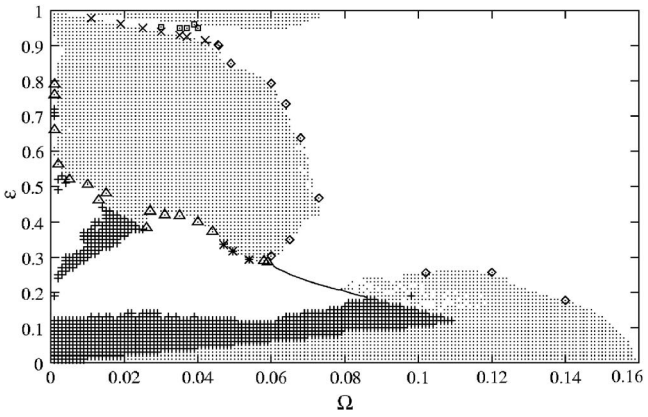

FIG. 1. The phase diagram for the coupled sine circle map lattice evolved using random initial conditions. The spatiotemporally synchronized solutions are represented by dots. The points at which DP exponents have been obtained are marked by diamonds ($\diamond$). At points marked with triangles ($\triangle$), SI with quasiperiodic bursts is seen. SI with TW bursts is seen at points marked by crosses ($\times$) and SI with period-5 bursts is seen at points marked with asterisks (*). STI with TW laminar states and solitons is seen at the points marked by boxes ($\square$). The cluster solutions are marked with plus (+) signs.

We study the system with random initial conditions. The system is updated synchronously with periodic boundary conditions in the parameter regime $0 \leqslant \Omega \leqslant \frac{1}{2\pi}$ and $K=1$ (where the single circle map has temporal period 1 solutions in this regime); the coupling strength ϵ is varied from 0 to 1.

The phase diagram obtained using random initial conditions is shown in Fig. 1 [21]. Spatially synchronized, temporally frozen solutions, where the variables $x_i(t)$ take the value $x_i(t)=x^\star=\frac{1}{2\pi}\sin^{-1}\frac{2\pi\Omega}{K}$ for all $i=1,\ldots,N$, and for all t, are marked by dots in Fig. 1. These solutions are seen over a large section of the phase diagram and are stable against perturbations. Cluster solutions, in which $x_i(t)=x_j(t)$ for all i,j belonging to a particular cluster, are identified by plus signs (+) in the phase diagram. Regimes of spatiotemporal intermittency of various kinds are seen near the bifurcation boundary of the synchronized solutions. The various types of STI seen are

(i) STI of the type in which the laminar state is the synchronized fixed point $x^\star$ defined earlier, and the turbulent state takes all other values other than $x^\star$ in the $[0,1]$ interval, is seen at points marked with diamonds ($\diamond$) in Fig. 1. The space-time plot is shown in Fig. 2(a). This type of STI belongs to the directed percolation universality class.

(ii) STI with TW laminar state interspersed with turbulent bursts is seen at points marked with boxes ($\square$) in Fig. 1. The space-time plot of this type of solutions is shown in Fig. 2(b). Coherent structures traveling in space and time are seen in these solutions. Such structures have also been seen in the Chaté-Manneville CML and have been called solitons in the literature.

(iii) Spatial intermittency with synchronized laminar state and quasiperiodic bursts are seen at parameters marked

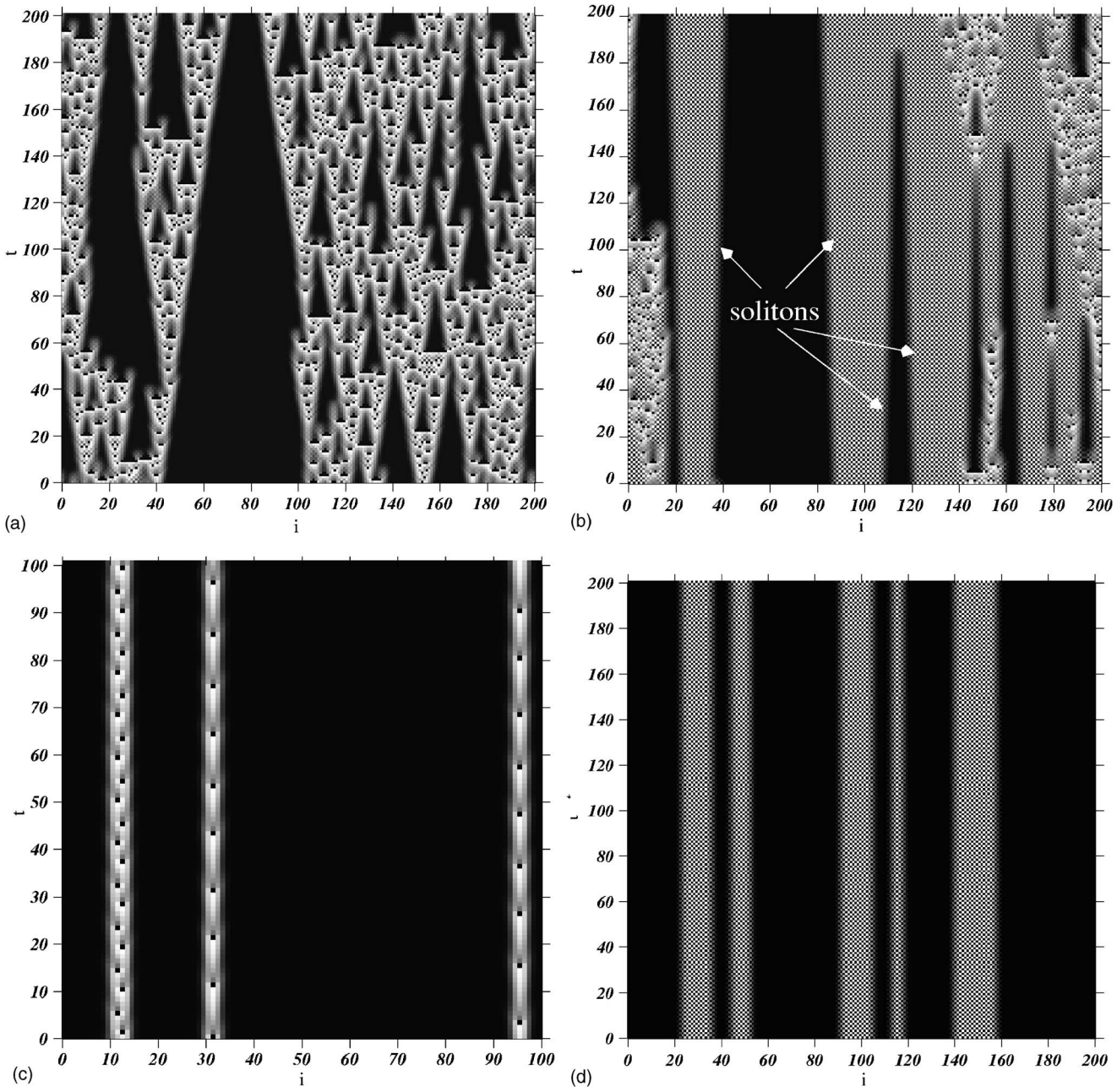

FIG. 2. The space-time plots of the different types of STI seen in the phase diagram. The lattice index i is along the x axis and the time index t is along the y axis. The space-time plots show (a) STI with synchronized laminar state interspersed with turbulent bursts seen at $\Omega=0.06$, $\epsilon=0.7928$. (b) STI with TW laminar state and turbulent bursts with solitons seen at $\Omega=0.037$, $\epsilon=0.937$. (c) SI with synchronized laminar state and quasiperiodic bursts seen at $\Omega=0.031$, $\epsilon=0.42$. (d) SI with synchronized laminar state and TW bursts observed at $\Omega=0.019$, $\epsilon=0.9616$.

with triangles ($\triangle$) in the phase diagram. The space-time plot of this type of solution is shown in Fig. 2(c).

(iv) Spatial intermittency with synchronized laminar state and traveling wave (TW) bursts are seen at points marked with crosses ($\times$) in the phase diagram. The space-time plot is shown in Fig. 2(d). SI with synchronized laminar state and period-5 bursts are seen at points marked with asterisks (*) in the phase diagram.

The identification of the universality classes of the different types of intermittency seen in this system has been partially carried out earlier. STI with synchronized laminar states and turbulent bursts has been clearly established to belong to the directed percolation (DP) class [17,18]. However, the other types of intermittency seen in the parameter space do not belong to the DP class. We analyze these in the next section.

III. UNIVERSALITY CLASSES IN THE SYSTEM

It is interesting to note that the system under study exhibits spatiotemporal intermittency belonging to a distinct universality class at different values of the parameters. The two

TABLE I. The static and dynamic exponents obtained in the DP regime at three of the points marked with diamonds ($\diamond$) in the phase diagram are shown in the above table. The universal DP exponents are listed in the last row. The exponents β and ν have been calculated using the hyperscaling relations. The data have been collected for a 1000 site lattice and are averaged over 1000 initial conditions. The definitions of the DP exponents are given in the Appendix .

Static and dynamic scaling exponents for the STI of the DP class										
		Bulk exponents						Spreading exponents		
Ω	$\epsilon_c(\Omega)$	z	$\beta/\nu z$	β	ν	η'	ζ	η	δ	z_s
0.060	0.7928	1.59	0.17	0.293	1.1	1.51	1.68	0.315	0.16	1.26
0.073	0.4664	1.58	0.16	0.273	1.1	1.50	1.65	0.308	0.17	1.27
0.065	0.34949	1.59	0.16	0.273	1.1	1.50	1.66	0.303	0.16	1.27
Error bars		0.01	0.01			0.01	0.01	0.001	0.01	0.01
DP		**1.58**	**0.16**	**0.28**	**1.1**	**1.51**	**1.67**	**0.313**	**0.16**	**1.26**

distinct classes obtained so far are regimes of STI which belong to the DP class and regimes of SI which do not belong to the DP class. We discuss each of these in further detail.

A. STI of the DP type

It has been shown convincingly that STI with synchronized laminar state interspersed with turbulent bursts (seen at points marked with $\diamond$ in Fig. 1) belongs to the DP universality class [17,18]. The infective dynamics of the turbulent bursts wherein the turbulent site either infects the adjacent laminar sites, or dies down to the laminar state, is similar to the behavior seen in directed percolation [22]. Since no spontaneous creation of turbulent bursts takes place, the laminar state forms the absorbing state and time acts as the directed axis. The entire set of static and dynamic scaling exponents obtained in this parameter regime match with the DP exponents which are defined in the Appendix. The exponents obtained, after averaging over 10^3 initial conditions, at three such parameter values are listed in Table I. The complete set of exponents and their definitions have been reported in Refs. [17,18]. The distribution of laminar lengths also shows a scaling behavior of the form $P(l) \sim l^{-\zeta}$, with an associated exponent, $\zeta \sim 1.67$. The laminar length distribution obtained, after averaging over 50 initial conditions, at $\Omega=0.06$, $\epsilon=0.7928$ has been plotted in Fig. 3(a). The size of the lattice studied was 10^4.

A clean set of DP exponents is obtained for the STI with synchronized laminar state seen in this parameter regime as these regimes are completely free from the presence of coherent solitonlike structures which could bring in long-range correlations in the system and thereby spoil the DP behavior. In fact, in the case of the STI with synchronized laminar state, no solitons have been observed for this model in the range of parameters studied. However, the STI with traveling wave laminar states seen at the parameter values marked with boxes in the phase diagram does show the presence of solitons as seen in the space-time plot of Fig. 2(b). These solitons could be responsible for nonuniversal exponents and crossover behavior in this regime. This behavior is discussed in detail in Sec. IV. In the remainder of the present section we will discuss the second universality class seen for the present model, viz. that of spatial intermittency.

B. Spatial intermittency

We now discuss the other type of intermittency, seen in this system viz. spatial intermittency. Spatial intermittency is a distinct class of STI in which the temporal behavior of both the laminar and burst states is regular. The infective dynamics characteristic of the DP class is absent here, and the burst states do not infect the laminar states even when they are nearest neighbors. Spatial intermittency is a long lived phenomenon and the spatially intermittent state persists for time scales which are much longer than the time scales on which the STI states die down to a uniform laminar background. Two different types of spatial intermittency have been seen in this system. In both types of SI, the laminar state is the synchronized fixed point $x^\star$ defined earlier. However, the burst states are different and may be either quasiperiodic (marked by triangles in the phase diagram) or periodic in their temporal behavior.

1. SI with quasiperiodic bursts

Spatial intermittency, in which the temporal behavior of the burst states is quasiperiodic in nature, has been seen at points marked with triangles ($\triangle$) in Fig. 1. The space-time plot has been shown in Fig. 2(c). These burst states are noninfective in nature, i.e., the probability of the burst state infecting the nearby laminar state is zero. Therefore the laminar states remain laminar forever. Hence, after an initial transient, the order parameter of the system, which is defined as the fraction of nonlaminar sites in the lattice, is a constant. The time series of the burst states at different parameter values, at a typical burst site, was studied using power spectrum analysis. The power spectrum obtained at $\Omega=0.058$, $\epsilon=0.291$ and $\Omega=0.0495$, $\epsilon=0.3178$ has been shown in Fig. 4. As can be seen from Fig. 4(a), the peaks are seen at ω_1, ω_2, $\omega_1+\omega_2$, and at $m\omega_1+n\omega_2$. This kind of behavior is typical of a quasiperiodic state. Hence we confirm that a quasiperiodic burst state is seen at $\Omega=0.058$, $\epsilon=0.291$.

The laminar length distribution of this type of SI shows a scaling behavior of the form $P(l) \sim l^{-\zeta}$ with an associated exponent $\zeta \sim 1.1$. The laminar length distribution at param-

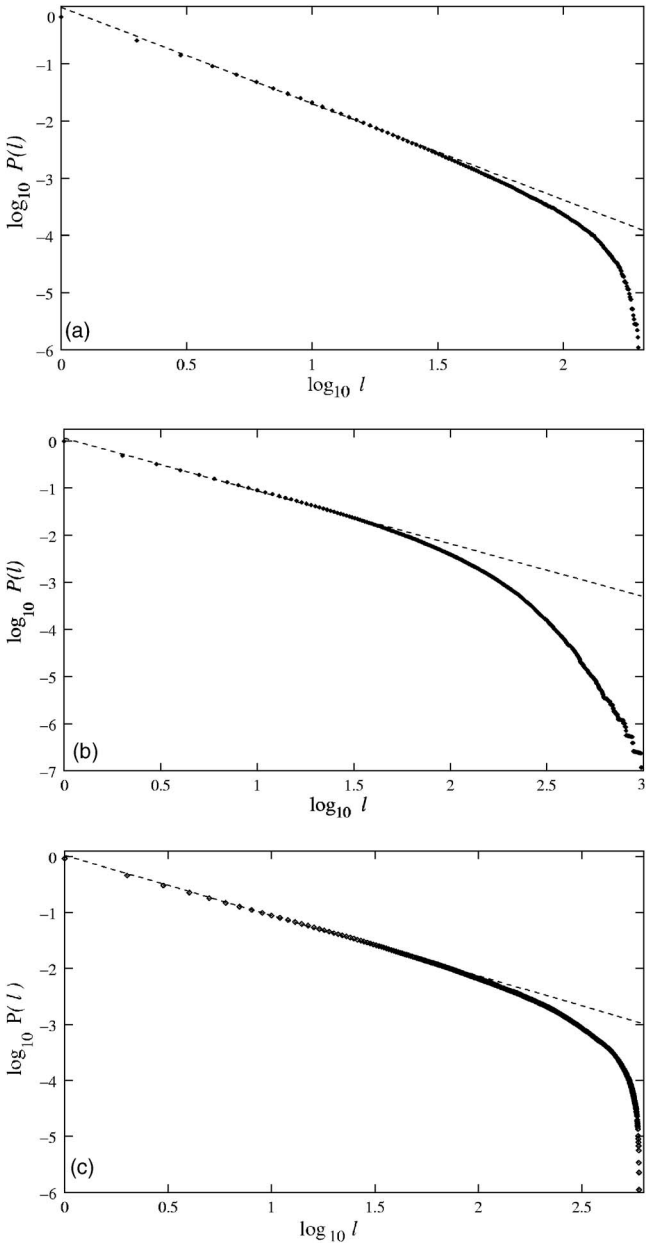

FIG. 3. The log-log (base 10) plot of the laminar length distribution for (a) STI of the DP class obtained at $\Omega=0.06$, $\epsilon=0.7928$. The exponent ζ is 1.681. (b) SI with quasiperiodic bursts obtained at $\Omega=0.04$, $\epsilon=0.402$. The exponent ζ is 1.10. (c) SI with TW bursts obtained at $\Omega=0.019$, $\epsilon=0.9616$. The exponent obtained is 1.08. The data have been obtained for a 10^4 site lattice and are averaged over 50 initial conditions.

eters ($\Omega=0.04$, $\epsilon=0.402$) has been plotted in Fig. 3(b). The values of ζ obtained for this type of SI at different values of (Ω,ϵ) have been listed in Table II. The scaling exponent ζ obtained for this type of SI is clearly different from that of the DP class ($\zeta_{DP}=1.67$).

Second, the transition to SI from a completely synchronized state is a first order transition unlike the transition to STI belonging to the directed percolation class which shows a second order transition. This can be seen in Fig. 5(a) in which the order parameter of the system m, which is defined

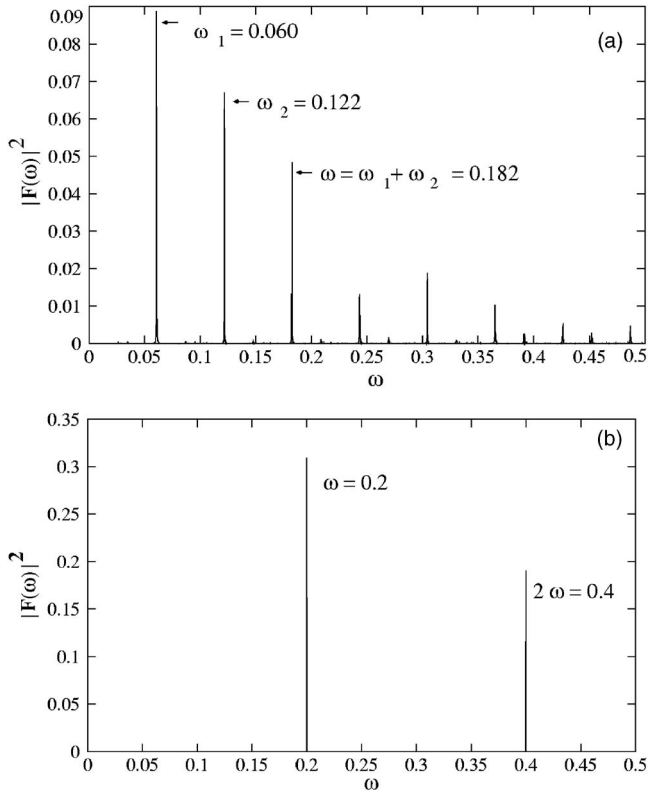

FIG. 4. The power spectrum $|F(\omega)|^2$ of the time series of the burst state seen at (a) $\Omega=0.058$, $\epsilon=0.291$ and (b) $\Omega=0.0495$, $\epsilon=0.3178$. The time series shown in (a) exhibits quasiperiodic behavior and the time series shown in (b) is periodic in nature.

as the fraction of burst states in the lattice, has been plotted as a function of the coupling strength ϵ. The order parameter m increases continuously with ϵ in the case of STI of the DP class, signalling a second order transition, whereas m shows a sharp jump with ϵ in the case of SI with quasiperiodic bursts, indicating that a first order transition takes place in the case of SI.

TABLE II. The table shows the laminar length distribution exponent ζ calculated for SI with quasiperiodic bursts [marked by triangles (△) in Fig. 1] for a lattice of size $N=10^4$ and averaged over 50 initial conditions. The exponent κ is the exponent associated with the number of gaps, $N_g(l)\sim l^{-\kappa}$ in the eigenvalue distribution, where l is the bin size chosen. The frequencies, ω inherent in the time series of the burst state are also listed and are of the form ω_1, ω_2, and $\omega_1+\omega_2$.

Spatial intermittency with quasiperiodic bursts				
Ω	ϵ	ζ	κ	ω
0.005	0.520	1.08±0.01	1.07±0.01	0.007, 0.014, 0.022
0.010	0.505	1.13±0.01	1.06±0.01	0.027, 0.054, 0.081
0.015	0.480	1.11±0.03	1.14±0.02	0.037, 0.073, 0.110
0.035	0.418	1.10±0.05	1.43±0.03	0.110, 0.230, 0.340
0.040	0.402	1.10±0.04	1.31±0.01	0.150, 0.230, 0.380
0.044	0.373	1.09±0.03	1.18±0.03	0.060, 0.120, 0.180
0.059	0.286	1.16±0.02	1.07±0.02	0.066, 0.133, 0.200

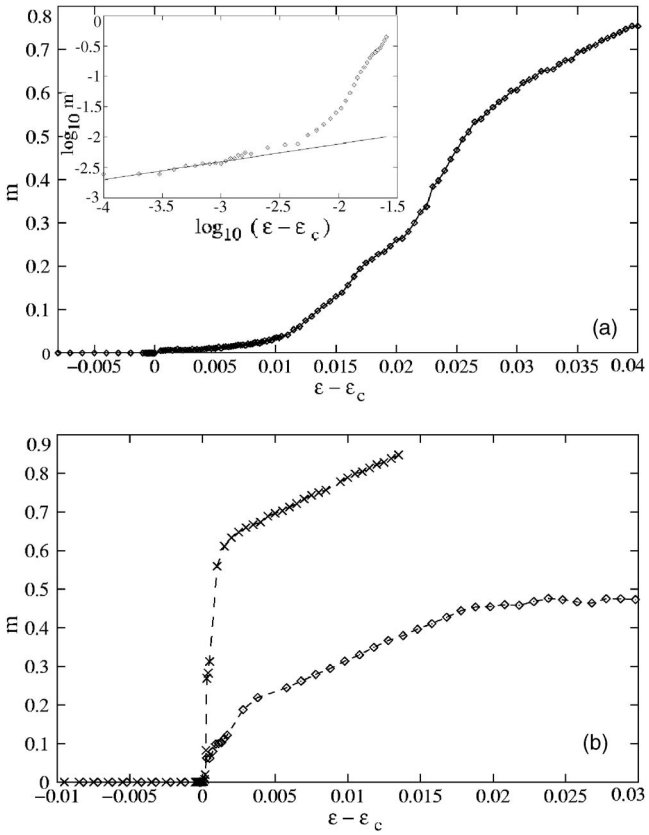

FIG. 5. The order parameter m vs $(\epsilon-\epsilon_c)$ plotted for STI of the DP class at $\Omega=0.06$ in (a). The inset figure shows the log-log (base 10) plot of m vs $(\epsilon-\epsilon_c)$. The exponent obtained is $\beta=0.296\pm0.027$. (b) shows m vs $(\epsilon-\epsilon_c)$ plotted for SI with TW bursts at $\Omega=0.042$ $(\times)$ and SI with quasiperiodic bursts at $\Omega=0.031$ $(\diamond)$. SI shows a first order transition whereas DP class shows a second order transition. The data have been collected for a 5000 site lattice and are averaged over 1000 initial conditions.

2. SI with periodic bursts

Spatial intermittency with periodic bursts forms the second class of SI. Two distinct burst periods have been observed in the phase diagram. Bursts of period 5 have been seen at the points marked by asterisks (*) in the phase diagram.

Figure 4(b) shows that peaks are seen in the power spectrum of the burst state time series at $\omega=0.2$ and higher harmonics. This confirms that the burst states have period 5 at $\Omega=0.0495$, $\epsilon=0.3178$, which is one of the points marked by asterisks in the phase diagram.

Bursts of spatial period 2, temporal period 2, of the traveling wave (TW) type are seen at the points marked by crosses $(\times)$ in the phase diagram. The laminar state in both cases is the spatiotemporally synchronized fixed point $x^\star$. The space-time plot of these SI with TW burst solutions at $\Omega=0.019$, $\epsilon=0.9616$ is shown in Fig. 2(d). The bursts are noninfective in nature in this type of SI as well. The scaling exponent, ζ associated with the laminar length distribution at different parameter values in this regime have been listed in Table III for both TW and period-5 bursts. The laminar length distribution exponent obtained in this regime is

TABLE III. The table shows the laminar length distribution exponent ζ calculated for SI with periodic bursts [marked by crosses $(\times)$ and asterisks (*) in Fig. 1] for a lattice of size $N=10^4$ and averaged over 50 initial conditions. The exponent κ is the exponent associated with the number of gaps, $N_g(l)\sim l^{-\kappa}$ in the eigenvalue distribution, where l is the bin size chosen. The frequencies ω inherent in the time series of the burst state are also listed.

Spatial intermittency with periodic bursts				
Ω	ϵ	ζ	κ	ω
0.019	0.9616	1.08±0.04	1.18±0.04	0.5
0.025	0.9496	1.08±0.02	1.12±0.02	0.5
0.037	0.9254	1.17±0.02	1.07±0.01	0.5
0.042	0.9148	1.13±0.02	1.10±0.04	0.5
0.047	0.3360	1.13±0.02	1.02±0.01	0.2, 0.4
0.0495	0.3178	1.15±0.04	1.03±0.02	0.2, 0.4
0.054	0.2936	1.17±0.03	1.02±0.02	0.2, 0.4

$\zeta\sim1.1$ (see Fig. 3). The transition to SI with TW burst state from a spatiotemporally synchronized state is also a first order transition as has been shown by the abrupt jump in the order parameter m with change in the coupling strength ϵ [Fig. 5(b)].

It is thus clear that SI does not belong to the DP universality class. The scaling exponent $\zeta=1.1$ for laminar lengths for the SI is distinctly different from the DP exponent $\zeta=1.67$. We note, however, that the nature of the bursts, viz. periodic or quasiperiodic, has no effect on the value of the exponent ζ. We hence conclude that SI with periodic as well as quasiperiodic bursts belong to the same class. A similar value of the laminar length distribution exponent $(\zeta\sim1.1)$ has been reported for spatial intermittency in the inhomogeneously coupled logistic map lattice [12]. Thus spatial intermittency appears to constitute a distinct universality class of the non-DP type.

Therefore two distinct universality classes of spatiotemporal intermittency, viz. directed percolation and spatial intermittency, are seen in the coupled sine circle map lattice in different regions of the parameter space. The reasons for the appearance of these two distinct classes may lie in the long-range correlations in the system at different parameter values.

IV. ROLE OF SOLITONS IN STI WITH TW LAMINAR STATE

As mentioned in Sec. III A, in addition to spatiotemporal intermittency with synchronized laminar states, the phase diagram of our model also shows spatiotemporal intermittency with TW laminar states and turbulent bursts at the points marked by boxes in the phase diagram. The lattice dies down to the absorbing TW laminar state from random initial conditions asymptotically. The STI with TW laminar states seen in this model appears as a result of a tangent-period doubling bifurcation from the SI with TW bursts as can be seen from Table IV.

TABLE IV. The largest positive and largest negative eigenvalues observed when SI with TW bursts (marked with crosses in the phase diagram) bifurcates to STI with TW laminar states (marked with boxes). The solution changes through a tangent-period doubling (TP) bifurcation.

Bifurcations from SI with TW bursts			
Ω	ϵ	Eigenvalues	Type of bifurcation
0.0100	0.982	1.685, −1.618	TP
0.0210	0.960	1.361, −1.222	TP
0.0305	0.943	1.752, −1.535	TP
0.0410	0.920	1.623, −1.309	TP

Immediately after the bifurcation, apart from turbulent states, coherent structures, which have been called solitons, are seen in the TW laminar background. These structures have been marked in the space-time plot of this type of STI in Fig. 2(b). The solitons travel through the lattice with a velocity $v=1/t'$ such that for a right moving soliton $x_i^t = x_{i+1}^{t+t'}$, and $x_i^t = x_{i-1}^{t+t'}$ for a left moving soliton. Here, i and t are the site and time indices, respectively. In this model, the left and right moving solitons occur in pairs and hence they annihilate each other. When these solitons collide, they either die down to the TW laminar state or give rise to turbulent bursts. Such coherent structures have been seen earlier in the Chaté-Manneville CML [14], where these solitons were responsible for spoiling the DP behavior and were even capable of changing the order of the transition.

Table V lists the laminar length exponents seen at different parameter values in the solitonic regime. The exponent values listed here vary from 1 to 1.5 at different points in the solitonic regime. Additionally, the escape time τ which is defined as the time taken for the lattice to relax to a completely laminar state, starting from random initial conditions, does not show power-law scaling as a function of L for any value of the parameters (see Fig. 6). It is possible that these apparently different exponents can be explained by scaling corrections, although the exponent values listed in the table are stable over lattice sizes from 2000 to 20 000 sites. On the other hand, the presence of solitons may contribute to genuinely nonuniversal behavior. This merits further investigation.

TABLE V. The laminar length distribution exponent ζ obtained for different values of the coupling strength ϵ and for different Ω's in the STI with TW laminar state and turbulent bursts regime. The data have been collected for a lattice of size $N=10^4$ and have been averaged over 50 initial conditions.

Laminar length exponents in the solitonic regime			
$\Omega=0.035$		$\Omega=0.037$	
ϵ	ζ	ϵ	ζ
0.933	1.53±0.01	0.930	1.50±0.02
0.943	1.40±0.01	0.937	1.31±0.05
0.950	1.17±0.01	0.950	1.17±0.01
0.962	1.02±0.01	0.962	1.02±0.00

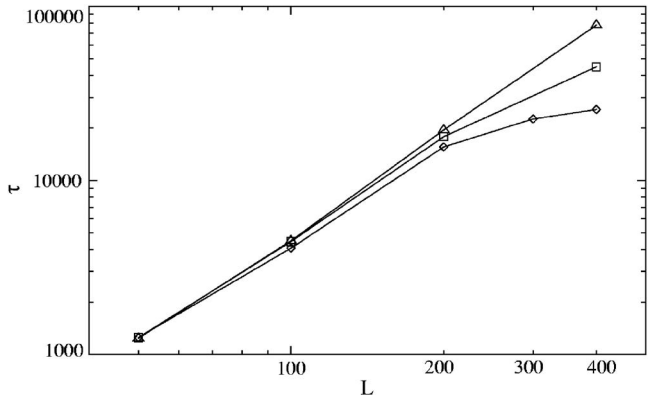

FIG. 6. The log-log (base 10) plot of escape time τ plotted as a function of the lattice size L at $\Omega=0.037$ and at $\epsilon=0.937$ (◇), 0.938 (□), and at $\epsilon=0.939$ (△). The data are averaged over 1000 initial conditions.

The soliton lifetimes and velocities depend on the coupling strength ϵ and Ω. The distribution of soliton lifetimes is shown in Fig. 7. As the coupling strength ϵ increases, the velocity v of the solitons is found to increase. Therefore solitons with larger velocities collide earlier with each other, and hence have shorter lifetimes. The distribution of soliton lifetimes shows a peak in the short lifetime regime indicating the presence of a characteristic soliton lifetime τ_c. However, the tail of the distribution falls off with power-law behavior with an exponent 2.84. For low values of ϵ, where the soliton velocities are smaller, there is no peak or characteristic lifetime in the distribution, and the entire distribution of soliton lifetimes scales as a power law with exponent ~1.1 (see Fig. 7). It is seen that the exponent ζ for the laminar lengths decreases as the lifetimes decrease and the turbulent spreading in the lattice decreases (see Table VI).

The spreading dynamics in this type of STI was studied by introducing a cluster of turbulent seeds in a completely absorbing background. The two dynamic quantities (i) $N(t)$ the fraction of turbulent sites in the lattice at a time t, and (ii) the survival probability $P(t)$, which is defined as the fraction of initial conditions at time t which show a nonzero number of active sites, were studied at $\Omega=0.035$ and $\epsilon=0.933$, 0.943, 0.95, and 0.962. These have been plotted in Figs. 8(a) and 8(b), respectively. It can be seen from the figure that the fraction of turbulent sites $N(t)$ at a given time t decreases as the coupling strength ϵ is increased. We see a similar decrease in the fraction of initial conditions which survive, $P(t)$ with increase in ϵ. The data are averaged over 1000 initial conditions.

Therefore we can conclude that the extent of spreading in the lattice decreases as the lifetime of the soliton decreases (with increase in ϵ). Since the distribution of laminar lengths is an indirect measure of the spreading in the lattice, we see that the varying average soliton lifetimes influence the distribution of laminar lengths and contribute to the existence of a variety of exponents here. Conversely, the soliton lifetime distributions have been plotted in Fig. 7(b) for parameters where the exponents ζ for the laminar length distributions

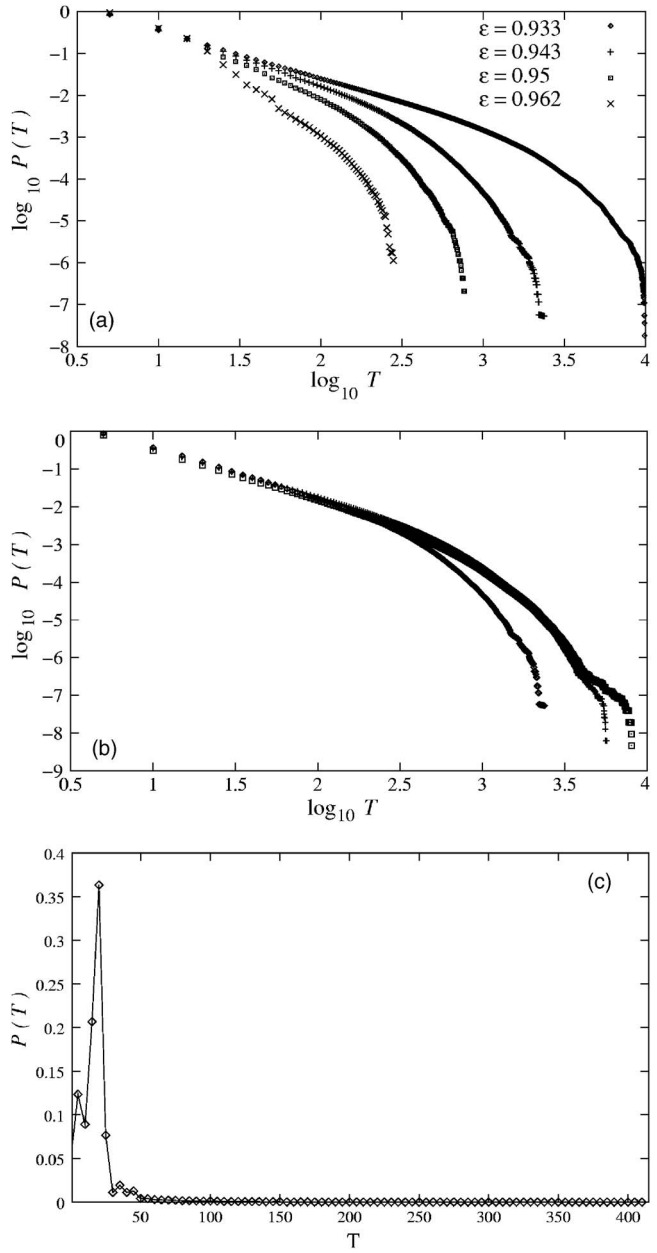

FIG. 7. (a) The log-log (base 10) plot of distribution of soliton lifetimes at $\Omega=0.035$ and at $\epsilon=0.933$ ($\zeta=1.53$), $\epsilon=0.943$ ($\zeta=1.40$), $\epsilon=0.95$ ($\zeta=1.14$), and at $\epsilon=0.962$ ($\zeta=1.02$). The exponent ζ depends on the soliton lifetimes. (b) The log-log (base 10) plot of the soliton lifetime distribution at $\Omega=0.035$, $\epsilon=0.943$ (diamonds); $\Omega=0.037$, $\epsilon=0.937$ (pluses), and at $\Omega=0.04$, $\epsilon=0.9323$ (boxes). The laminar length distribution exponent ζ is ~ 1.3 at all these points. Hence the soliton lifetimes collapse onto each other. (c) The soliton lifetime distribution seen in the short soliton lifetime regime at $\Omega=0.037$, $\epsilon=0.962$. A peak is seen at the characteristic time scale $\tau_c=20$. The distributions have been obtained after evolving a lattice of size 500 over 20 000 time steps and 50 initial conditions.

take similar values. The soliton lifetime distributions collapse over each other as expected.

We note again that the STI with TW laminar state shows no soliton free regime, and the DP regime where the laminar state is the synchronized state is completely soliton free.

TABLE VI. The exponents obtained in the short and long soliton lifetime regimes. Here, ζ is the laminar length distribution exponent. A characteristic time scale τ_c is seen in the short soliton lifetime regime. T_{max} is the largest soliton lifetime observed and μ is the exponent associated with the soliton lifetime distribution.

Soliton lifetimes in STI with TW laminar state						
Regime	Ω	ϵ	ζ	τ_c	T_{max}	μ
Long soliton lifetimes	0.035	0.933	1.53		19010	1.14
		0.943	1.40		2481	1.35
	0.037	0.930	1.50		16961	1.18
		0.937	1.31		5782	1.31
Short soliton lifetimes	0.035	0.962	1.02	15	305	2.84
	0.037	0.962	1.02	20	413	2.88

Hence no direct comparison of the exponents of the STI with synchronized laminar state and STI with TW laminar state is possible at present.

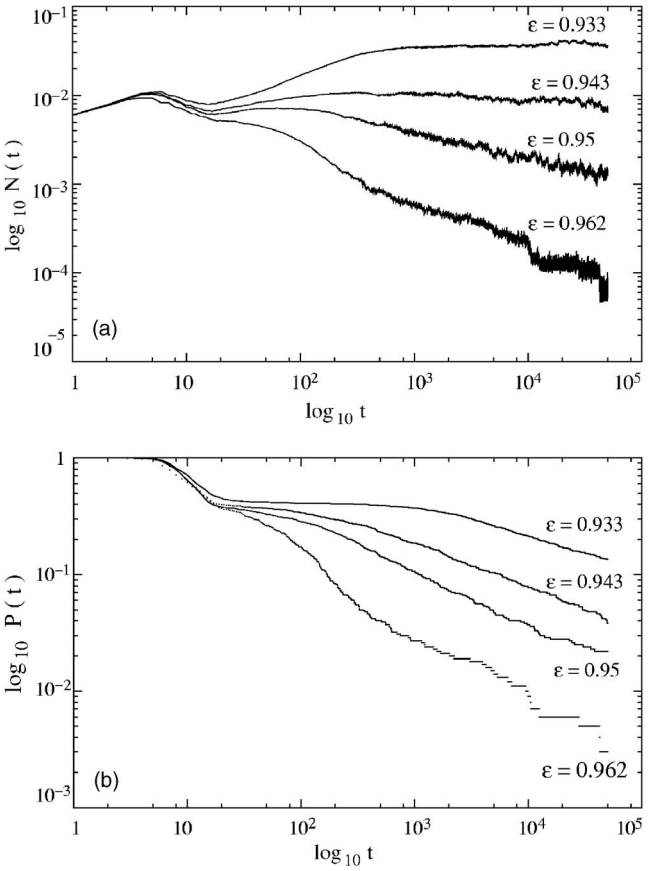

FIG. 8. The log-log plot of (a) the fraction of turbulent sites $N(t)$ plotted as a function of t at $\Omega=0.035$, and (b) the survival probability $P(t)$ plotted as a function of t at $\Omega=0.035$. The extent of spreading decreases with increasing coupling strength ϵ or equivalently with decreasing soliton lifetimes. The data has been obtained for a 1000 site lattice and has been averaged over 1000 initial conditions.

V. DYNAMIC CHARACTERIZERS

It has been seen earlier that the signature of the DP and non-DP behavior in this system can be seen in the dynamical characterizers of the system, specifically in the eigenvalues of the one-step stability matrix. Regimes of STI with DP behavior exhibited a continuous eigenvalue spectrum, whereas regimes of spatial intermittency showed an eigenvalue spectrum with level repulsion, where distinct gaps were seen in the spectrum.

The linear stability matrix of the evolution equation (1) at one time step about the solution of interest is given by the $N \times N$ dimensional matrix M_t^N, given below:

$$\mathbf{M_t^N} = \begin{pmatrix} \epsilon_s f'(x_1^t) & \epsilon_n f'(x_2^t) & 0 & \cdots & 0 & \epsilon_n f'(x_N^t) \\ \epsilon_n f'(x_1^t) & \epsilon_s f'(x_2^t) & \epsilon_n f'(x_3^t) & 0 & \cdots & 0 \\ 0 & \epsilon_n f'(x_2^t) & \epsilon_s f'(x_3^t) & \cdots & 0 & 0 \\ \vdots & \vdots & \vdots & \vdots & \vdots & \vdots \\ \epsilon_n f'(x_1^t) & 0 & \cdots & 0 & \epsilon_n f'(x_{N-1}^t) & \epsilon_s f'(x_N^t) \end{pmatrix},$$

where $\epsilon_s = 1-\epsilon$, $\epsilon_n = \epsilon/2$, and $f'(x_i^t) = 1 - K\cos(2\pi x_i^t)$. x_i^t is the state variable at site i at time t, and a lattice of N sites is considered. The diagonalization of the stability matrix gives the N eigenvalues at time t.

A. Eigenvalue distribution

The eigenvalue distribution $P(\lambda)$ of the matrix above, in all the cases studied here, have been obtained after averaging over 50 initial conditions for 1000 lattice sites. Figure 9 shows the eigenvalue distributions for STI belonging to DP class at the typical parameter value $\Omega = 0.06$, $\epsilon = 0.7928$ (a), SI with quasiperiodic bursts at the typical value $\Omega = 0.04$, $\epsilon = 0.402$ (b), and SI with TW bursts at $\Omega = 0.025$, $\epsilon = 0.9496$ (c). The bin size chosen is 0.005. It is clear from the figure that the eigenvalue distribution of the DP class at this value of bin size is continuous whereas distinct gaps can be seen in the distribution for the spatial intermittency class for both quasiperiodic and periodic bursts.

For the case of the SI, the number of vacant bins in the eigenvalue distribution $N_g(l)$ scales as a power law $N_g(l) \sim l^{-\kappa}$ where l is the bin size (Fig. 10). However, the exponent κ depends on the inherent dynamics of the burst states. The exponent κ for SI with quasiperiodic bursts have been listed in Table II and the exponents for SI with periodic bursts are listed in Table III.

Within the SI class, the value of κ is seen to be stable within each period for the periodic bursts (see Fig. 10). In the quasiperiodic case, the natural frequencies of the dynamics are different at different values of the parameter and hence κ values are different for different values of the parameters. It is also useful to track the temporal evolution of the largest eigenvalue to identify the signatures of the differences between these three cases.

B. Temporal evolution of the largest eigenvalue

The temporal evolution of the largest eigenvalue of the stability matrix λ_m with t contains information about the dynamical behavior of the burst states. The time series of the largest eigenvalue was obtained for the three cases: STI of the DP class, SI with quasiperiodic bursts, and SI with TW bursts. After the initial transient λ_m settles down to the natural periods of the burst states. The power spectrum $|F(\omega)|^2$ picks out the inherent frequencies in the system. This is evident from Fig. 11 in which the power spectrum of the time series of $\lambda_m(t)$ has been plotted as a function of the frequencies.

In the case of SI with QP bursts [Fig. 11(a)], peaks are seen at ω_1, ω_2, $\omega_1+\omega_2$, and at $m\omega_1+n\omega_2$ $(m,n>0)$ as is typical of a quasiperiodic behavior. However, in the case of STI of the DP class, a broadband spectrum is obtained which implies that the burst states contain many frequencies [Fig. 11(b)]. In the case of SI with periodic bursts, peaks are seen in the power spectrum at $\omega = 0.5$ for SI with TW bursts [Fig. 11(c)], indicating period-2 temporal behavior, whereas the peaks are seen at $\omega = 0.2$ and 0.4 for the type of SI in which the temporal behavior of the bursts is period 5.

Thus we note that DP behavior is associated with a broadband spectrum for the power spectrum of the temporal evolution of the largest eigenvalue, as well as a gapless distribution of eigenvalues, whereas the SI or non-DP behavior is associated with the characteristic power spectrum of the temporal nature of the burst states, i.e., periodic or quasiperiodic behavior, and distinct gaps in the eigenvalue distribution.

VI. CONCLUSIONS

Thus spatiotemporal intermittency of several distinct types can be seen in different regions of the phase diagram of the coupled sine circle map lattice. STI is seen all along the bifurcation boundaries of bifurcations from the synchronized solutions. These bifurcations are of the tangent-tangent (TT) and tangent-period doubling (TP) type. The universal behavior of the system as typified by the laminar length exponents is of two types—the directed percolation (DP) class and the non-DP class. STI with synchronized laminar states belongs

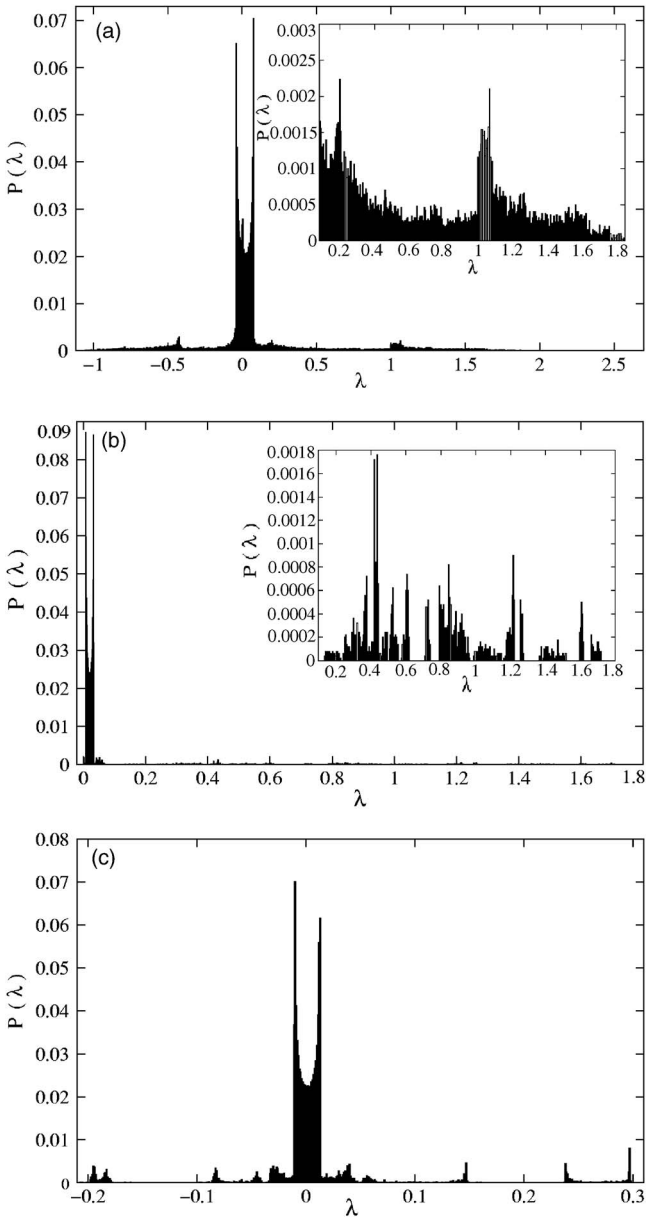

FIG. 9. The eigenvalue distribution (bin size=0.005) for (a) STI belonging to the DP class at $\Omega=0.06$, $\epsilon=0.7928$, (b) spatial intermittency with quasiperiodic bursts at $\Omega=0.04$, $\epsilon=0.402$, and (c) SI with TW bursts at $\Omega=0.025$, $\epsilon=0.9496$. A section of the eigenvalue distribution is magnified in the inset figures. Gaps are seen in the spatial intermittency eigenvalue distributions whereas the eigenvalue distribution for STI does not show any such gaps. The data have been obtained for a lattice of size $N=1000$ and have been averaged over 50 initial conditions.

convincingly to the DP class and can be seen after both TT and TP bifurcations from the synchronized state. This class of STI is remarkably free of the solitons which spoil the DP behavior in other models such as the Chaté-Manneville CML. Other regimes of the phase diagram show spatial intermittency (SI) behavior where the laminar regions show power-law scaling and are periodic in behavior, and the burst states show temporally regular behavior of the periodic and quasiperiodic type. This type of intermittency is clearly not

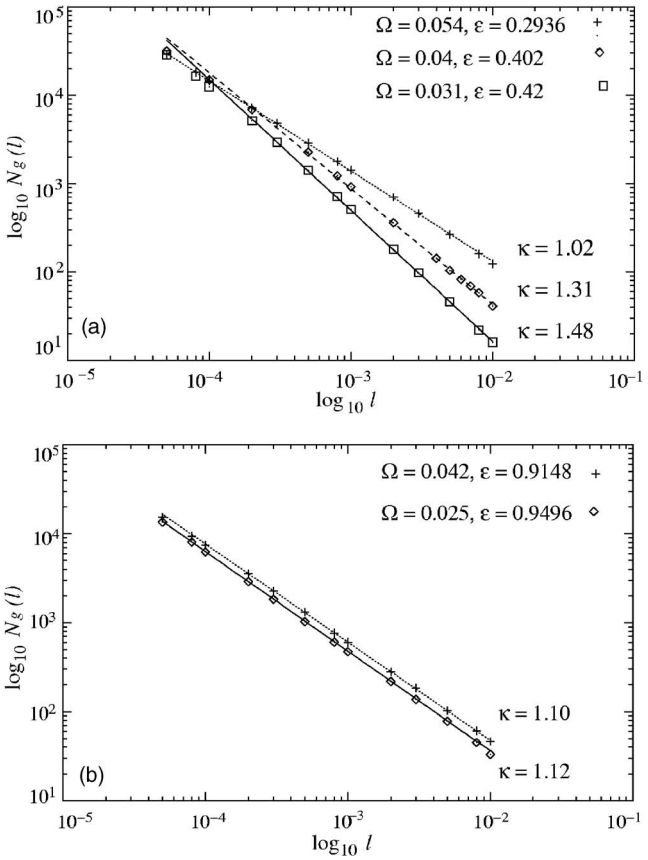

FIG. 10. The number of vacant bins $N_g(l)$ plotted against the bin size l on a log-log (base 10) scale for (a) SI with quasiperiodic bursts, and (b) SI with periodic bursts. The exponent κ associated with $N_g(l) \sim l^{-\kappa}$ is given in the figures.

of the DP type and has earlier been seen in the inhomogeneously coupled logistic map lattice.

In addition to the two regimes above, we also see STI with traveling wave (TW) laminar state in some regions of the parameter space. This kind of STI arises as the result of a TP bifurcation from SI with synchronized laminar state and TW bursts. This type of STI shows a variety of exponents. These exponents are stable over a range of lattice sizes and could arise due to scaling corrections, or to the presence of solitons. The soliton lifetimes depend on the parameter values and their distributions show two characteristic regimes. In the first regime, where typical lifetimes are short, the distribution peaks at short lifetimes showing the presence of a characteristic soliton lifetime scale but has a power-law tail. In the second regime, where soliton lifetimes are typically larger, the distribution has no characteristic scale and shows power-law behavior with an exponent in the range 1.1–1.2.

The dynamic characterizers of the system, namely, the eigenvalues of the stability matrix, shows signatures of these distinct types of behavior. The DP regime is characterized by a gapless eigenvalue distribution and a broadband power spectrum of the time series of the largest eigenvalue. For the SI case, i.e., the non-DP regime, distinct gaps are seen in the eigenvalue distribution, and the power spectrum of the temporal evolution of the largest eigenvalue is characteristic of periodic or quasiperiodic behavior depending on the temporal nature of the burst states.

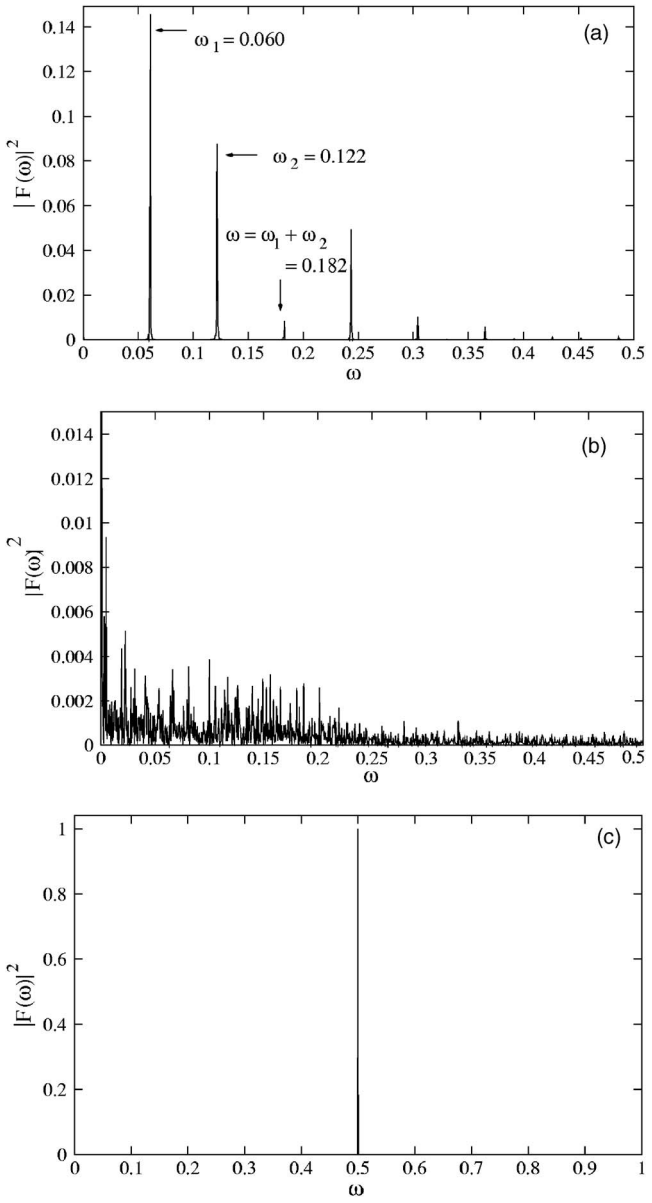

FIG. 11. The power spectrum of the time series of the largest eigenvalue $\lambda_m(t)$ at (a) Ω=0.058, ϵ=0.291, where SI with quasiperiodic behavior is seen, (b) Ω=0.06, ϵ=0.7928, where STI of the DP class is seen, and (c) Ω=0.026, ϵ=0.948, where SI with TW bursts is seen. Three main frequencies ω_1, ω_2, and $\omega_1+\omega_2$ are seen in (a) whereas, a broadband spectrum is seen in the case of STI of the DP class as seen in (b). The spectrum of SI with TW shows a peak at 0.5 as seen in (c).

The origin of the different types of universal behavior in different parameter regimes appears to lie in the long range correlations in the system. These correlations in the system appear to change character in different regimes of parameter space leading to dynamic behavior with associated exponents of the DP and non-DP types. In order to gain insight into the nature of the correlations in this system, and the way in which they change character in different parameter regimes, we plan to set up probabilistic cellular automata which exhibit similar regimes and to examine their associated spin Hamiltonians [23]. Absorbing phase transitions are seen in other CML's [24,25] and in pair contact processes [26–28]. Models of nonequilibrium wetting setup using contact processes with long-range interactions also show DP or non-DP behavior depending on the activation rate at sites at the edges of inactive islands [29]. Similar ideas may apply to the behavior in our model as well. Solid on solid models also show DP and non-DP transitions depending on specific forms of binding, i.e., transition rates of the dynamics [30]. These models are inspired by studies of the synchronization transition in CML's [31,32] where transitions like the Kardar-Parisi-Zhang transition are also seen. We hope to explore these directions in future work.

ACKNOWLEDGMENTS

Z.J. thanks CSIR, India, for financial support. N.G. thanks DST, India, for partial support.

APPENDIX: DEFINITION OF DP EXPONENTS

The DP transition is characterized by a set of static and dynamic critical exponents associated with various quantities of physical interest.

1. Static exponents

(i) We first consider the escape time $\tau(\Omega,\epsilon,L)$, which is defined as the time taken for the system starting from random initial conditions to relax to a completely laminar state. It is expected from finite-size scaling arguments that τ varies with the system size L such that

$$\tau(\Omega,\epsilon) = \begin{cases} \log L & \text{laminar phase} \\ L^z & \text{critical phase} \\ \exp L^c & \text{turbulent phase.} \end{cases}$$

Hence at the critical value of the coupling strength ϵ_c, the escape time τ shows a power-law behavior, z being the associated exponent.

(ii) The order parameter $m(t)$ associated with this transition is defined as the fraction of turbulent sites in the lattice at time t. At ϵ_c, the order parameter scales as

$$m \sim (\epsilon - \epsilon_c)^{\beta}, \quad \epsilon \to \epsilon^{+}. \tag{A1}$$

At $t \ll \tau$, $m(t)$ scales with t as $m(\epsilon_c,t) \sim t^{-\beta/\nu z}$, where ν is the exponent associated with the spatial correlation length.

The exponent ν is obtained by using the scaling relation

$$\tau(L,\epsilon_c) \sim \phi^z f(L/\phi), \tag{A2}$$

where ϕ is the correlation length which diverges as $\phi \sim \delta^{-\nu}$ and δ is given by $(\epsilon-\epsilon_c)$. Hence ν is adjusted until the scaled variables $L\delta^{\nu}$ and $\tau\delta^{\nu z}$ collapse onto a single curve.

(iii) The correlation function in space is defined as

$$C_j(t) = \frac{1}{L}\sum_{i=1}^{L} \langle x_i^t x_{i+j}^t \rangle - \langle x_i^t \rangle^2. \tag{A3}$$

At ϵ_c, $C_j(t)$ scales as $C_j(t) \sim j^{1-\eta'}$.

(iv) The distribution of laminar lengths $P(l)$ is an important characterizer of the universality class [11]. The laminar lengths l are defined as the number of laminar sites between two turbulent sites. At criticality, the laminar length distribution shows a power-law behavior of the form

$$P(l) \sim l^{-\zeta}. \tag{A4}$$

ζ is the associated exponent, ζ_{DP} being 1.67.

2. Dynamical exponents

To extract the dynamical exponents, two turbulent seeds are placed in an absorbing lattice and the spreading of the turbulence in the lattice is studied. The quantities associated with critical exponents at ϵ_c are as follows:

(i) The number of active sites $N(t)$ at time t, which scales as $N(t) \sim t^{\eta}$.

(ii) The survival probability $P(t)$ defined as the fraction of initial conditions which show a nonzero number of active sites at time t. This scales as $P(t) \sim t^{-\delta}$.

(iii) The radius of gyration $R^2(t)$, which is defined as the mean squared deviation of the position of active sites from the original sites of turbulent activity. This scales as $R^2(t) \sim t^{z_s}$.

[1] S. Ciliberto and P. Bigazzi, Phys. Rev. Lett. **60**, 286 (1988).
[2] F. Daviaud, M. Bonetti, and M. Dubois, Phys. Rev. A **42**, 3388 (1990).
[3] P. W. Colovas and C. D. Andereck, Phys. Rev. E **55**, 2736 (1997).
[4] P. Rupp, R. Richter, and I. Rehberg, Phys. Rev. E **67**, 036209 (2003).
[5] S. M. Fielding and P. D. Olmsted, Phys. Rev. Lett. **92**, 084502 (2004).
[6] M. Das, B. Chakrabarti, C. Dasgupta, S. Ramaswamy, and A. K. Sood, Phys. Rev. E **71**, 021707 (2005).
[7] C. Pirat, A. Naso, Jean-Louis Meunier, P. Maissa, and C. Mathis, Phys. Rev. Lett. **94**, 134502 (2005).
[8] H. Chaté and P. Manneville, Phys. Rev. Lett. **58**, 112 (1987).
[9] H. Chaté, Nonlinearity **7**, 185 (1994).
[10] *Theory and Applications of Coupled Map Lattices*, edited by K. Kaneko (Wiley, New York, 1993).
[11] H. Chaté and P. Manneville, Physica D **32**, 409 (1988).
[12] A. Sharma and N. Gupte, Phys. Rev. E **66**, 036210 (2002).
[13] Y. Pomeau, Physica D **23**, 3 (1986).
[14] P. Grassberger and T. Schreiber, Physica D **50**, 177 (1991).
[15] T. Bohr, M. van Hecke, R. Mikkelsen, and M. Ipsen, Phys. Rev. Lett. **86**, 5482 (2001).
[16] J. Rolf, T. Bohr, and M. H. Jensen, Phys. Rev. E **57**, R2503 (1998).
[17] T. M. Janaki, S. Sinha, and N. Gupte, Phys. Rev. E **67**, 056218 (2003).
[18] Z. Jabeen and N. Gupte, Phys. Rev. E **72**, 016202 (2005).
[19] G. R. Pradhan and N. Gupte, Int. J. Bifurcation Chaos Appl. Sci. Eng. **11**, 2501 (2001); G. Pradhan, N. Chatterjee, and N. Gupte, Phys. Rev. E **65**, 046227 (2002).
[20] N. Chatterjee and N. Gupte, Phys. Rev. E **53**, 4457 (1996).
[21] Z. Jabeen and N. Gupte, in *Proceedings of the First National Conference on Nonlinear Systems and Dynamics*, NCNSD-2003, ITT-Kharagpur, December 2004, pp. 101–104 (eprint nlin.CD/0502053).
[22] D. Stauffer and A. Aharony, in *Introduction to Percolation Theory* (Taylor and Francis, London, 1992).
[23] E. Domany and W. Kinzel, Phys. Rev. Lett. **53**, 311 (1984).
[24] P. Marcq, H. Chaté, and P. Manneville, Phys. Rev. Lett. **77**, 4003 (1996).
[25] P. Marcq, H. Chaté, and P. Manneville, Phys. Rev. E **55**, 2606 (1997).
[26] J. Kockelkoren and H Chaté, Phys. Rev. Lett. **90**, 125701 (2004).
[27] H. Hinrichsen, Physica A **361**, 457 (2006).
[28] G. Ódor, Rev. Mod. Phys. **76**, 663 (2004); Phys. Rev. E **70**, 066122 (2004).
[29] F. Ginelli, H. Hinrichsen, R. Livi, D. Mukamel, and A. Politi, Phys. Rev. E **71**, 026121 (2005).
[30] A. Lipowski and M. Droz, Phys. Rev. E **68**, 056119 (2003).
[31] M. Droz and A. Lipowski, Phys. Rev. E **67**, 056204 (2003).
[32] A. S. Pikovsky and J. Kurths, Phys. Rev. E **49**, 898 (1994).